Marine and Petroleum Geology 137 (2022) 105498

Contents lists available at ScienceDirect

Marine and Petroleum Geology

journal homepage: www.elsevier.com/locate/marpetgeo

The porosity preserving effect of basin wide illitic coating in deeply buried sandstone intervals of the lower Jurassic Stø Formation, Barents Sea

Kristoffer Løvstad *, Henrik Nygaard Hansen, Jens Jahren

University of Oslo, Department of Geosciences, Sem Sælands Vei 1, 0371, Oslo, Norway

ARTICLE INFO

Keywords:
Southwestern barents sea
Stø formation
Grain coating clay minerals
Illitic coating
Reservoir quality
Porosity preservation
Diagenesis

ABSTRACT

The Stø Formation contains the main target reservoirs for petroleum exploration in the Norwegian Barents Sea Area, however, the clean sandstones of the Stø Formation can be heavily quartz cemented in areas that have undergone extensive post depositional burial. The Stø Formation in well 7219/8-2 has previously been identified as having porosities well above the expected porosity depth trend due to the porosity preserving effects of illitic grain coating. In this study the Stø Formation in 14 wells with maximum burial depths at top of formation ranging from 2672 to 3623 m have been investigated and several new intervals of the formation show abnormally high porosities relative to the expected burial trend. Thin sections from 4 wells were available and in all of these remnants of grain coating illitic clay was observed in varying amounts, with the effectiveness in reducing quartz cement overgrowth being determined by the continuity of grain coats. This indicates that the degree of grain coating coverage exerts the main control on the porosity of the clean deeply buried parts of the Stø Formation. With increasing burial depths, the porosity difference between intervals with continuous grain coats and intervals with less continuous grain coats becomes ever larger. Intervals observed to have extensive grain coating coverage compact with a significantly reduced rate with increasing burial compared to poorer coated intervals in the chemical compaction domain. The noticeable and consistent difference in the chemical compaction trend between coated- and negligible coated intervals within the Stø Formation could allow for establishment of powerful predictive models without the need for expensive petrographic- or core plug data.

1. Introduction

The oil and gas industry is to an increasing degree shifting their focus towards deeply buried reservoir prospects, and the predictability of reservoir quality in these prospects is therefore becoming ever more important.

The Stø Formation is present across most of the Norwegian Barents Sea and the formation is an important target for petroleum exploration (Worsley et al., 1988). The Stø Formation has in places been subjected to considerable maximum burial depths, up to 3623 m in the studied wells e.g. Baig et al. (2016). The mainly clean homogenous sandstones of the Stø Formation (Olaussen et al., 1984), may thus have been subjected to extensive quartz overgrowth causing significantly lowered porosities. Previously grain coating clay minerals, from hereon called grain coats, of sufficient extent to limit quartz cementation have been seen to preserve porosities well above the porosity depth trend in the Stø Formation. This was mainly seen in intervals interpreted to be of an upper shoreface facies that was deposited in periods of relative quiescence compared to other sections of the Stø Formation (Hansen et al., 2017).

During mechanical compaction the amount of porosity lost with increasing burial is governed by the sediments textural and mineralogical composition e.g., (Bjørlykke et al., 1989; Lundegard, 1992; Chuhan et al., 2002; Paxton et al., 2002; Marcussen et al., 2010), but if the sediments are subjected to temperatures above 70–80 °C, precipitation of silica becomes a significant factor (McBride, 1989; Bjørlykke and Egeberg, 1993). The amount of chemical compaction (quartz cementation) is a function of the time temperature integral (TTI) (Walderhaug, 1994). TTI reflect the burial curve/temperature history, including uplift within the chemical compaction domain. Quartz cement is considered to be the most important factor controlling porosity distribution in deep clean sandstone reservoirs (Bjørlykke and Egeberg, 1993). Grain coats if present on a large part of the detrital grain surface have the ability to reduce the amount of quartz cement precipitated by reducing the surface area available for nucleation of authigenic quartz (Heald and Larese, 1974). Variations in the degree of grain coating coverage will result in different responses to increasing burial in regard to the amount of

* Corresponding author.
E-mail address: krislovs@mail.uio.no (K. Løvstad).

https://doi.org/10.1016/j.marpetgeo.2021.105498
Received 3 February 2021; Received in revised form 9 December 2021; Accepted 20 December 2021
Available online 22 December 2021

porosity lost due to quartz cement in otherwise similar sands (Ajdukiewicz and Lander, 2010) (Fig. 1). Grain coats preserving porosity well above expected levels from average porosity depth trends have been discussed in several papers from the Norwegian continental shelf, mainly from the North Sea and the Norwegian Sea (Ehrenberg, 1993; Aase et al., 1996; Ramm et al., 1997; Bjørlykke, 1998; Jahren and Ramm, 2000; Maast et al., 2011), but recently also from the Barents Sea and Svalbard areas (Haile et al., 2018; Line et al., 2018). Microquartz and authigenic chlorite coating have primarily been found to preserve porosity. Albeit less often seen, Storvoll et al. (2002) also found illite or illite/chlorite coating to reduce precipitation of quartz cement.

Matlack et al. (1989) showed experimentally that infiltration of muddy waters can be an effective way of emplacing clay particles as coating on detrital sand grains. With high volumes of suspended clay along with fluctuating water levels yielding the most significant amount of grain coating clay minerals. Other studies have reported bioturbation as a factor in the emplacement of detrital clay on sand grains either by sand grains passing through the digestive systems of organisms or facilitated by the burrowing action of organisms (Wilson, 1992; Needham et al., 2005). Some studies have also shown estuaries to be a suitable for the formation of precursor grain coats (Wooldridge et al., 2017a, 2017b; Griffiths et al., 2018; Virolle et al., 2019) where the emplacement of clay coatings could be due to extracellular polymeric substances that are secreted by microorganisms and forming a biofilm that causes clay particles to attach to sand sized grains (Wooldridge et al., 2017a).

Remnants of inherited grain coats where seen in all our samples from the Stø formation indicating that previous emplacement of grain coats is common, but only extensively preserved in certain intervals (Hansen et al., 2017). Previously the research on the Stø Formation has mostly been focused on provenance and the depositional processes, the regional structural and general sedimentological makeup of the formation, e.g., (Olaussen et al., 1984; Gjelberg et al., 1987; Worsley et al., 1988; Bergan and Knarud, 1993b; Klausen et al., 2018, 2019). In this study our prime objective is therefore to investigate the regional occurrence of grain coating illitic clay and its control on the porosity distribution in deeply buried parts of the Stø Formation.

2. Geological setting

The Stø Formation was deposited during late Pliensbachian to Bajocian times. The formation is a part of the Realgrunnen subgroup (Norian – Bajocian) where it overlies the Nordmela Formation consisting of interbedded sandstone, siltstone, mudstone and claystone, overlying the Stø Formation is the Fuglen Formation consisting of pyritic mudstones with interbedded limestone (Fig. 2). The Stø Formation generally consists of medium to very fine-grained mature sandstones that are moderately to well sorted. The Stø Formation is highly condensed and consists mainly of shallow marine sandstone deposited in an overall prograding coastal regime with several transgressive events interrupting the overall trend marked by thin siltstone and shale layers (Olaussen et al., 1984; Gjelberg et al., 1987; Worsley et al., 1988; Klausen et al., 2018).

The quartz content of the Stø Formation is generally around 91–100% of the detrital grains (Bergan and Knarud, 1993a). The mature nature of the formation is due to both the shallow marine depositional environment yielding a high amount of sediment reworking (Worsley, 2008), and the mature source area of the rejuvenated hinterland in the south (Bergan and Knarud, 1993a; Ryseth, 2014; Line et al., 2020). Furthermore Klausen et al. (2019) found a tectonically induced change in provenance within the Stø Formation, from reworked Triassic sediments in the lower part of the formation to mature sediments coming from the Caledonides in the upper part, with this altered tectonic setting causing not only a shift in provenance area but also a concurrent shift in the depositional setting. From more tidally influenced transgressive lags in the lower part of the formation to more fluvial influenced deposits in the upper part (Klausen et al., 2018). Table 1 shows the present depth to top Stø Formation as well as the estimated maximum burial depth of the formation, most likely reached in Eocene or Oligocene (Baig et al.,

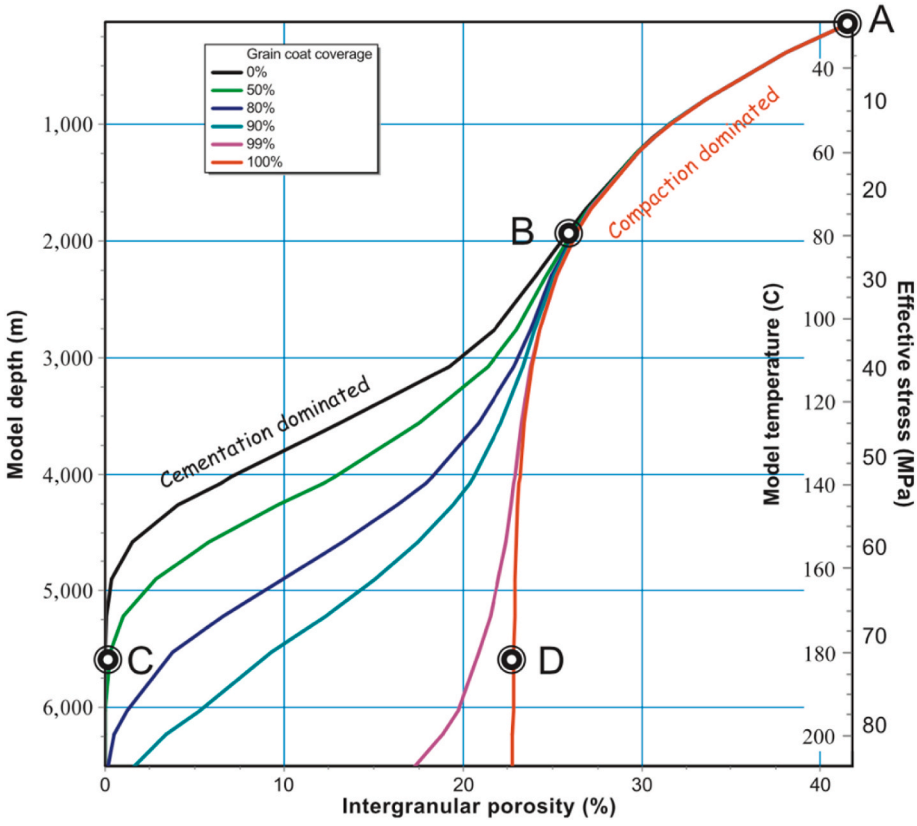

Fig. 1. Porosity evolution with burial for a well-sorted, fine-grained, rigid-grained quartzo-feldspathic eolian sandstone with variable grain coat coverage. A sand deposited with an initial porosity of 42% (A) undergoes subsidence to a depth of 6200 m over a period of 155 m.y. with no uplift or overpressure development. In this example porosity decrease by means of mechanical compaction to a depth of 2 km, at this point (B) the porosity is 26%. From this point further mechanical compaction in rigid-grained sandstones continues at an exceptionally low rate (red curve). When temperatures increase to above 70–80 °C quartz cement can precipitate, with the rate of precipitation mainly determined by the time temperature integral and quartz grain surface area available for nucleation of quartz cement. Grain coats limit this surface area and with increasing burial depth the variation in porosity between differently coated sands becomes ever increasing (e.g., C to D). Figure from Ajdukiewicz and Lander (2010). (For interpretation of the references to color in this figure legend, the reader is referred to the Web version of this article.)

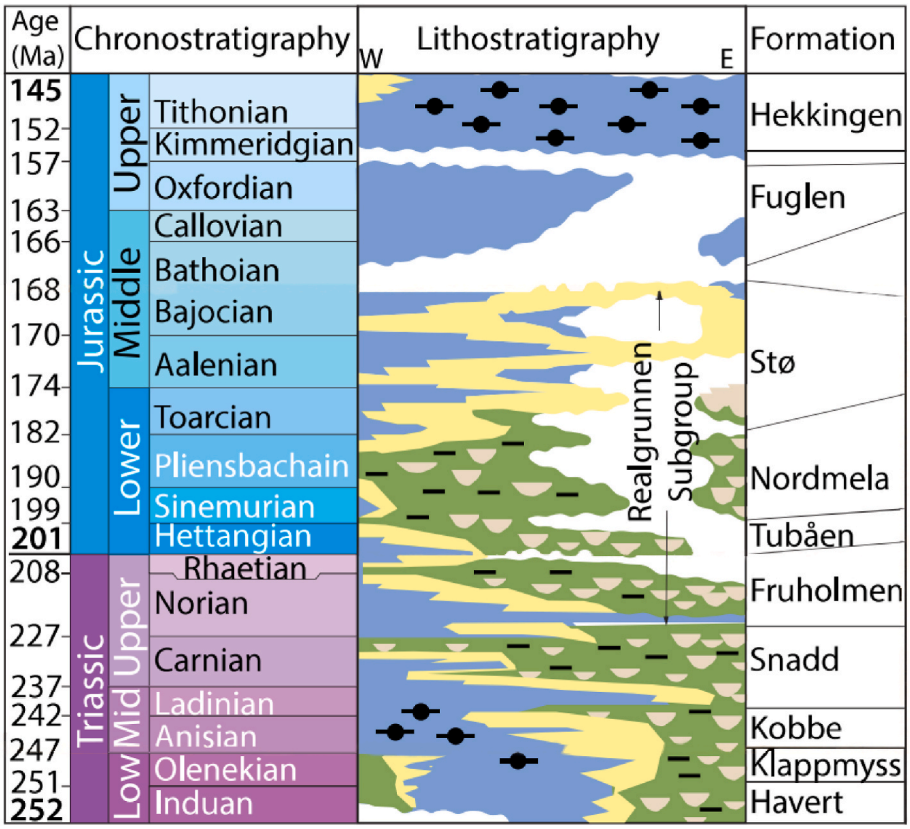

Fig. 2. Chrono- and lithostratigraphy chart of Triassic and Jurassic successions in the SW Barents Sea. Figure from Müller et al. (2019).

2016). The amount of uplift varies across the Southwestern Barents Sea and ranges from 850 m to 1100 m in the studied wells. The Stø Formation in all studied wells have reached burial depths corresponding to temperatures well above what is required for the precipitation of quartz cement (Table 1).

The locations of the studied wells are shown on the map in Fig. 3. The wells are situated in the Bjørnøyrenna Fault complex, west of the Polhem subplatform, in the Ringvassøy-Loppa fault complex, west of the Hammerfest Basin and in addition, 10 of the wells are situated in the Hammerfest Basin. In the Hammerfest Basin one well is in the Northwestern

Table 1
General well information. *Maximum burial are based on Baig et al. (2016). Temperature estimates are based on the current geothermal gradient. All values are calculated at the top of formation. Temperatures in brackets for well 7120/5–1 and 7120/12–2 are the authors' estimate of a more realistic temperature gradient.

Well name	7119/9-1	7119/12-1	7120/2-3 S	7120/5-1	7120/6-1	7120/6-2 S	7120/12-2
Location	71° 24′ 53.19″ N 19° 49′ 43.26″ E	71° 6′ 8″ N 19° 47′ 40.29″ E	71° 47′ 20.97″ N 20° 21′ 44.23″ E	71° 34′ 51.86″ N 20° 26′ 12.26″ E	71° 37′ 11.76″ N 20° 55′ 59.72″ E	71° 36′ 0.6″ N 20° 49′ 41.7″ E	71° 7′ 30.3″ N 20° 48′ 19″ E
TVD	3248	3087	2620	2699	2820	3035	4667
Bottom hole temperature [°C]	112	96	93	66	104	111	115?
Geothermal gradient [°C]	35.7	32.1	39	26? (35)	40.3	39.8	24.8? (35)
Stø Formation [mRKB]	2748–2868	2658-3087?	2071–2221	2285–2427	2386–2470	2564–2678	1892–1978
Estimated uplift*	850	850	1150	1000	1100	1000	1000
Maximum burial depth [MD from surface]	3598	3283	2885.5	2967	3149	3220	2703
Maximum burial temperature [°C]	128.5	105.5	112.4	77.3? (103.8)	126.8	128	67? (94.6)
Present day temperature [°C]	98.1	78.2	67.6	51.2? (80)	82.5	88.3	42.2? (66)

Well name	7121/4-1	7121/4-2	7121/5-1	7121/5-2	7122/6-1	7219/8-2	7219/9-1
Location	71° 35′ 59.68″ N 21° 9′ 22.79″ E	71° 39′ 26.09″ N 21° 3′ 45.96″ E	71° 34′ 51.86″ N 20° 26′ 12.26″ E	71° 40′ 20.79″ N 21° 39′ 24.42″ E	71° 38′ 19.32″ N 22° 48′ 42.8″ E	72° 19′ 17.55″ N 19° 35′ 21.28″ E	72° 24′ 0.78″ N 19° 57′ 11.68″ E
TVD	2609	2798.5	3197	2540	2707	3413	4286
Bottom hole temperature [°C]	88	95	115	85	89	122	145
Geothermal gradient [°C]	37.3	37	39.1	37	37.2	38.8	36.1
Stø Formation [mRKB]	2318–2396	2480–2557	2369–2445	2323–2400	2015–2038	2898–2985	1951–2062
Estimated uplift*	925	925	1000	1100	1100	1100	1100
Maximum burial depth [MD from surface]	2886	3066	3011	3073	2691	3623	2672
Maximum burial temperature [°C]	107.6	113.4	117.7	113.7	100.2	140.7	96.4
Present day temperature [°C]	73.1	79.2	78.6	73	59.2	98	56.7

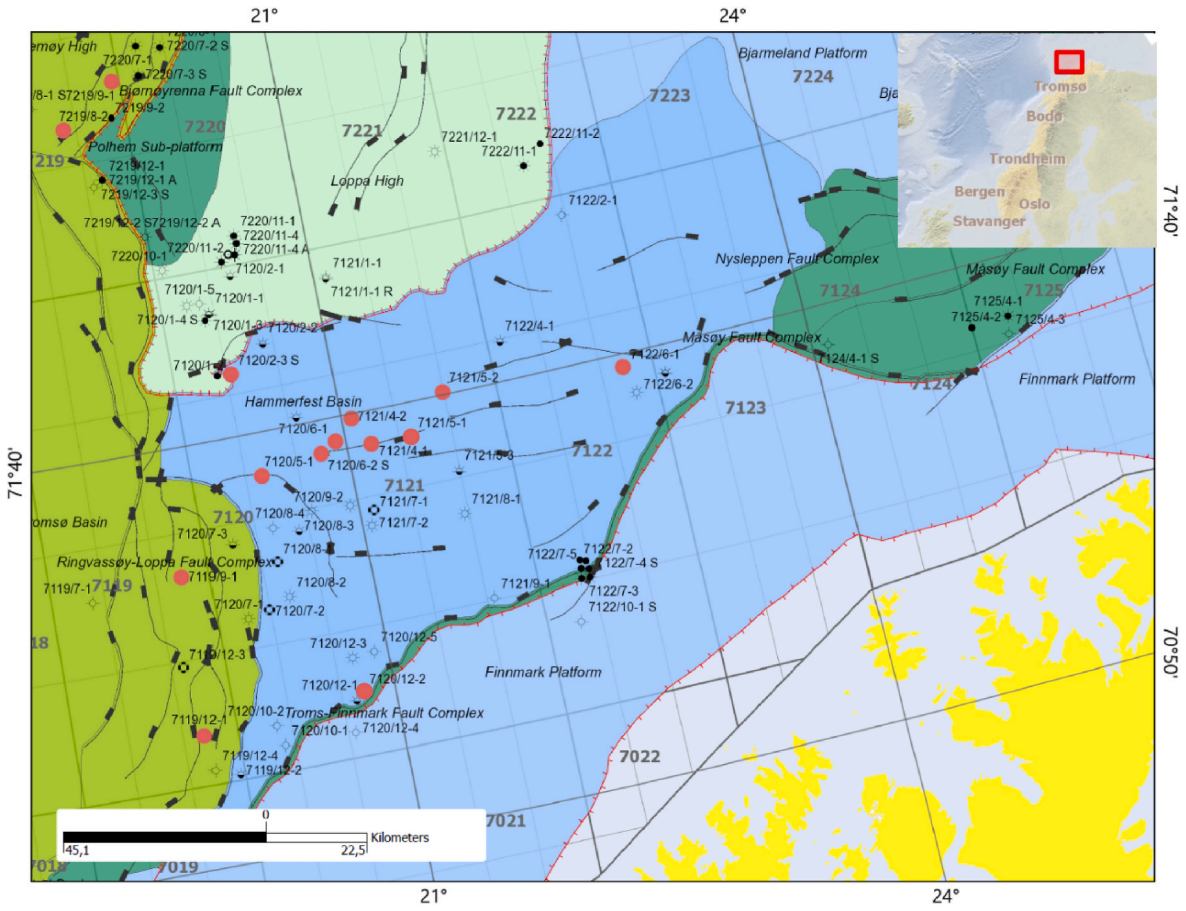

Fig. 3. Position of the studied wells in the Southwestern Barents Sea on a structural map (Norwegian Petroleum Directorate FactMap, retrieved August 27, 2018 from http://gis.npd.no/factmap).

corner of the basin on the boundary towards the Loppa high, two are in the Southwestern corner on the boundary to the Finnmark Platform and the remainder of the wells are in the middle of the basin, mainly in the western parts.

3. Methods and data

Coreplug- and petrophysical data from 14 wells formed the basis for this study (Table 1). In addition point count data from 4 wells were available, well 7219/8–2 from Hansen et al. (2017), and 3 additional new wells point counted for this study) (Table 2). The petrographic database consists of 38 thin section samples where the mineralogical distribution was determined by analogue point counting of each sample using a Nikon Eclipse 50/pol optical microscope. Textural parameters were obtained by measuring grain sizes in the Infinity Analyze software using an optical microscope fitted with a camera.

The thin sections available were point counted with 300 points counted per sample. The longest axis was measured on >100 randomly picked detrital grains. Sorting calculations were performed using the method defined by Folk and Ward (1957). Thin sections were inspected in a Hitachi SU5000 scanning electron microscope (SEM) using back-scattered electrons (BSE) and energy dispersive spectroscopy (EDS). SEM analysis was used to detect and analyze the composition and appearance of grain coatings. The grain coats was not recognizable in the optical microscope. This was due to the grain coats being both exceedingly thin and because of its morphology. The grain coating minerals were situated tangentially on the grain surfaces. Had the clay coating minerals been situated radially on the grain surfaces it may still have been possible to differentiate the coating in the optical microscope using cross polarized light and looking for the interference color of the illite. Thus, it was not possible to obtain a quantitative measure of the degree of grain coating coverage. Instead, a qualitative classification was made on all samples studied in SEM, determining the visual extent of the grain coats. All depths mentioned are in meters below rotary table (mRKB) unless otherwise stated. Maximum burial depth estimates are based on the uplift map in Baig et al. (2016). Maximum temperatures at the top of the Stø Formation are based on the present-day geothermal gradient as calculated from the recorded bottom hole temperature (BHT). Note that temperatures shown for the Stø Formation in the wells 7120/12–2 and 7120/5–1 are too low, this is most likely the result of erroneous BHT measurements. The geothermal gradients in the 7120/12–2 and 7120/5–1 wells are much more likely similar to those recorded in nearby wells. The amounts of quartz cement observed in parts of the formation in these two wells are also a strong indication that the temperature estimates are much too low. Porosity estimations were done in Interactive Petrophysics (IP) and consisted of neutron-density measurements corrected for shale volume, shale density, shale porosity, pore fluids and resistivity. The porosity estimation was quality checked against core plug measurements of horizontal helium porosity. For all the wells included in this study, core-plug measurements of porosity and permeability were available with a sample spacing of approximately 30 cm. Similar intervals of the Stø Formation in different wells were identified by characteristic petrophysical parameters facilitating an easy comparison and the ability to easily discriminate based on fixed values. Different intervals were defined primarily by the amount of shale (Vshale), porosity, P-wave sonic velocity (Vp) and density. The Vshale estimates were averaged from gamma ray and neutron-density calculation and performed uniquely for each well.

Table 2
Point count results. The colors in the SEM column denotes observed coating green: significant coating, red: negligible.

Point count results											Additional data			
Well	Sample [MD]	Quartz grains [%]	Feldspar grains [%]	Rock fragments [%]	Muscovite [%]	Tot. Clay [%]	Quartz cement [%]	Kaolinite [%]	Carbonate cement [%]	Porosity [%]	Mean grain size[mm]	Sorting [phi]	IGV [%]	SEM
7121/5-1	2372.9	63.00	0.00	0.33	2.67	6.67	16.33	0.67	1.67	8.67	0.09	0.37	34.00	
7121/5-1	2378.15	67.00	0.00	0.00	0.67	6.00	17.33	0.33	2.33	6.33	0.08	0.36	32.33	
7121/5-1	2382.12	67.67	0.67	0.00	0.00	3.67	16.67	0.00	2.00	9.33	0.09	0.37	31.67	
7121/5-1	2387.92	68.67	0.67	0.00	0.00	7.00	12.00	0.00	2.67	9.00	0.10	0.50	30.67	
7121/5-1	2410.28	70.67	0.67	0.33	0.33	2.33	9.67	1.00	1.33	13.67	0.18	0.49	28.00	
7121/5-1	2421.8	76.00	0.67	0.00	0.00	2.33	7.00	0.67	0.67	12.67	0.13	0.42	23.33	
7121/5-1	2426.25	70.00	1.33	0.67	0.00	4.00	7.00	0.33	1.33	15.33	0.13	0.34	28.00	
7120/6-1	2391.22	64.00	1.33	0.67	2.33	3.67	18.00	2.00	1.00	7.00	0.10	0.34	31.67	
7120/6-1	2395.74	73.00	0.67	1.33	0.00	1.33	8.33	0.33	2.00	13.00	0.12	0.38	25.00	
7120/6-1	2397.77	69.67	0.33	0.33	0.00	3.33	11.33	0.33	1.00	13.67	0.16	0.68	29.67	
7120/6-1	2400.43	72.33	0.67	0.67	0.00	1.67	7.00	0.00	1.00	16.67	0.22	0.42	26.33	
7120/6-1	2408.75	62.00	1.33	1.33	0.33	5.00	20.67	0.00	3.33	6.00	0.10	0.35	35.00	
7120/6-1	2415.25	63.00	1.33	0.67	0.67	9.00	14.33	0.00	3.00	8.00	0.09	0.35	34.33	
7120/6-1	2416.2	66.33	0.33	0.33	0.33	7.67	13.00	0.00	2.67	9.33	0.10	0.32	32.67	
7120/6-1	2422.44	72.33	1.00	0.67	0.00	5.33	12.33	0.00	1.67	6.67	0.12	0.34	26.00	
7120/6-1	2435.16	74.67	0.33	0.00	0.00	4.33	4.67	0.00	2.00	14.00	0.23	0.54	25.00	
7120/6-1	2446.26	77.00	1.00	0.00	0.00	1.00	4.67	0.00	0.33	16.00	0.17	0.38	22.00	
7120/6-1	2449.2	78.00	1.33	0.00	0.33	1.67	4.67	0.00	0.33	13.67	0.19	0.54	20.33	
7120/6-1	2461.8	76.00	1.67	0.00	0.00	2.67	4.00	0.33	0.00	15.33	0.18	0.54	22.33	
7120/2-3S	2078.70	79.00	0.00	0.00	0.33	1.00	3.33	0.00	0.33	16.00	0.13	0.42	20.67	
7120/2-3S	2099.72	68.67	1.33	0.00	1.00	11.67	10.00	0.67	0.00	6.67	0.07	0.51	29.00	
7120/2-3S	2109.33	70.67	1.00	0.00	0.00	8.00	8.67	0.33	0.00	11.33	0.09	0.45	28.33	
7120/2-3S	2132.65	71.00	0.00	0.00	0.00	4.00	7.00	0.67	0.00	17.33	0.16	0.42	29.00	
7120/2-3S	2140.60	74.33	0.00	0.67	0.00	1.33	7.00	0.00	0.00	16.67	0.16	0.42	25.00	
7120/2-3S	2146.80	72.00	1.67	0.00	0.00	3.00	7.00	1.00	0.00	15.33	0.13	0.50	26.33	
7120/2-3S	2153.36	78.00	0.33	0.33	0.00	1.67	7.33	0.67	0.00	11.67	0.16	0.53	21.33	
7120/2-3S	2159.75	75.67	0.33	0.33	0.00	4.67	6.33	0.00	0.00	12.67	0.14	0.47	23.67	
7219/8-2	2908.50	69.00	0.00	0.67	0.33	3.67	20.00	0.67	2.33	3.33	0.17	0.47	30.00	
7219/8-2	2912.50	68.30	0.00	0.00	0.00	2.60	21.30	1.00	0.60	6.00	0.19	0.35	31.50	
7219/8-2	2913.50	75.50	0.00	0.00	0.00	1.00	10.25	0.25	0.00	13.00	0.24	0.41	24.50	
7219/8-2	2914.00	71.00	0.00	0.33	0.00	3.00	10.00	0.33	1.33	14.00	0.29	0.52	28.67	
7219/8-2	2947.50	71.00	0.00	0.33	0.33	1.67	6.67	1.33	8.67	10.00	0.15	0.38	28.33	
7219/8-2	2953.50	64.00	0.00	0.33	1.00	4.67	22.67	1.00	3.33	3.00	0.16	0.36	34.67	
7219/8-2	2955.50	70.33	0.00	0.00	0.33	4.00	10.33	1.67	3.33	10.00	0.22	0.68	29.33	
7219/8-2	2957.50	71.67	0.67	0.00	0.00	2.00	5.33	1.00	2.00	17.33	0.26	0.55	27.67	
7219/8-2	2959.50	74.67	0.67	0.67	0.00	1.00	6.33	0.00	1.67	15.00	0.24	0.52	24.00	
7219/8-2	2961.50	70.33	0.00	0.33	0.00	0.67	11.33	0.33	2.00	15.00	0.21	0.42	29.33	
7219/8-2	2970.48	69.00	0.00	0.00	0.00	3.67	10.67	3.33	0.00	13.33	0.20	0.33	31.00	

4. Results

4.1. Petrographic results

The Stø Formation can be classified as a quartz arenite in all physical samples investigated in this study (Table 2). Percentages listed are in relation to total bulk volume. The quartz content ranges from 62 to 79% of the bulk volume and the feldspar and rock fragment content accounts for less than 2% each. Muscovite grains were also observed in all samples, but the amount is typically less than 1%. The pore-filling detrital clay content is highly variable ranging from approximately 1-12%. SEM analyses indicate that the pore-filling clay consists of illitic clay, occasionally with deformed lithic grains consisting of illite and microquartz incorporated in the matrix. Illitic clay was also observed in the SEM as grain coats on detrital quartz grains in several samples (Fig. 4 A - F), and each sample selected for SEM analysis was characterized. The exceedingly thin grain coats means that any volumetric percentage is impossible to determine, but as the degree of coating coverage is the governing factor on the ability of grain coats to limit quartz cement a qualitative approach were used to characterize the samples (red = negligible coating, if grain coats are present, it is only seen as remnants. green = coated sample, a large portion of the detrital grain surface is coated) (See Table 2). The results indicate that samples with a higher porosity tend to be more significantly coated compared to samples with low porosity (Table 2). Furthermore, in samples characterized as negligible grain coated, the clay fraction was predominantly observed as being pore-filling (Fig. 4G–I)). The authigenic cements observed in the studied samples are kaolinite-, carbonate- and quartz cement. The kaolinite- and carbonate cement are far less volumetrically significant compared to the quartz cement, ranging between approximately 0-4% and 0–9% respectively. The carbonate-cemented intervals are easily recognized in the sonic log with significantly higher Vp values. The quartz cement content is highly variable between individual samples and reaches approximately 23% in the most heavily cemented samples and as low as 3% in samples where quartz cement is limited (e.g., comparing Figs. 5C and 4D). The intergranular porosity observed in these samples is highly variable and ranges from approximately 3 to 17% (Fig. 4 and Table 2).

4.2. Grain coating illitic clay

Grain coats are present to some degree in all samples investigated, but with varying extent and thickness (Fig. 4). EDS spectra shows that the grain coats in all the samples contain potassium, aluminum, silica and oxygen, which along with the textural appearance indicate a mainly illitic composition (Matlack et al., 1989; Dutton and Diggs, 1992). In samples determined to be significantly coated most of the detrital grains

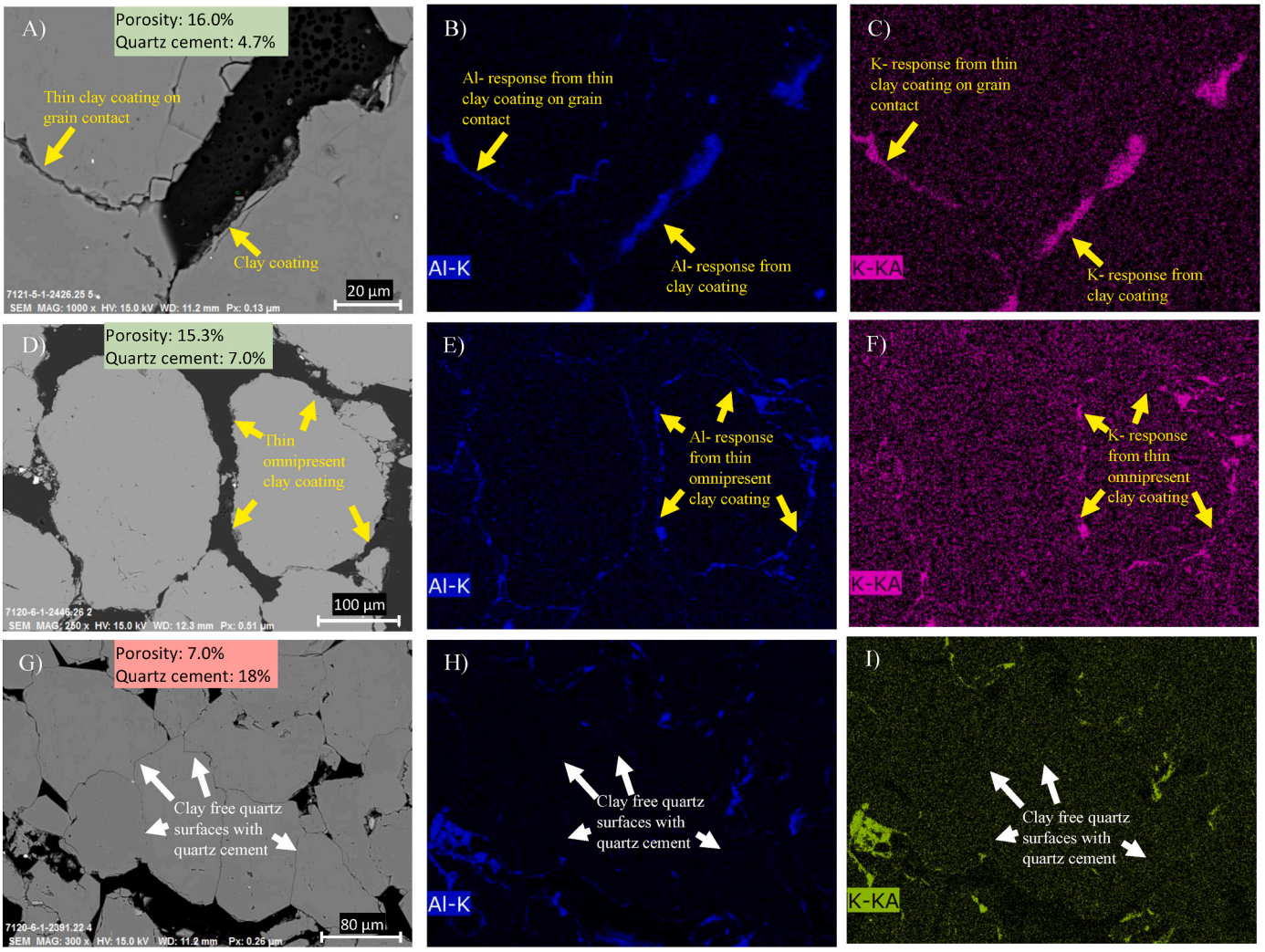

Fig. 4. Backscatter SEM micrographs from three different thin section samples with accompanying elemental maps showing the aluminum (Al)- and potassium (K) response of the area shown in the backscatter micrographs on the left. The thin clay coating is best seen in the Al-map. The potassium map indicate that the clay coating has an illitic composition. A-C) from well 7120/6–1, sample 2446.50. D-F) from well 7120/6–1, sample 2446.26. G-I) from well 7120/6–1, sample 2391.22. Note that remnants of clay coatings are present on some grains.

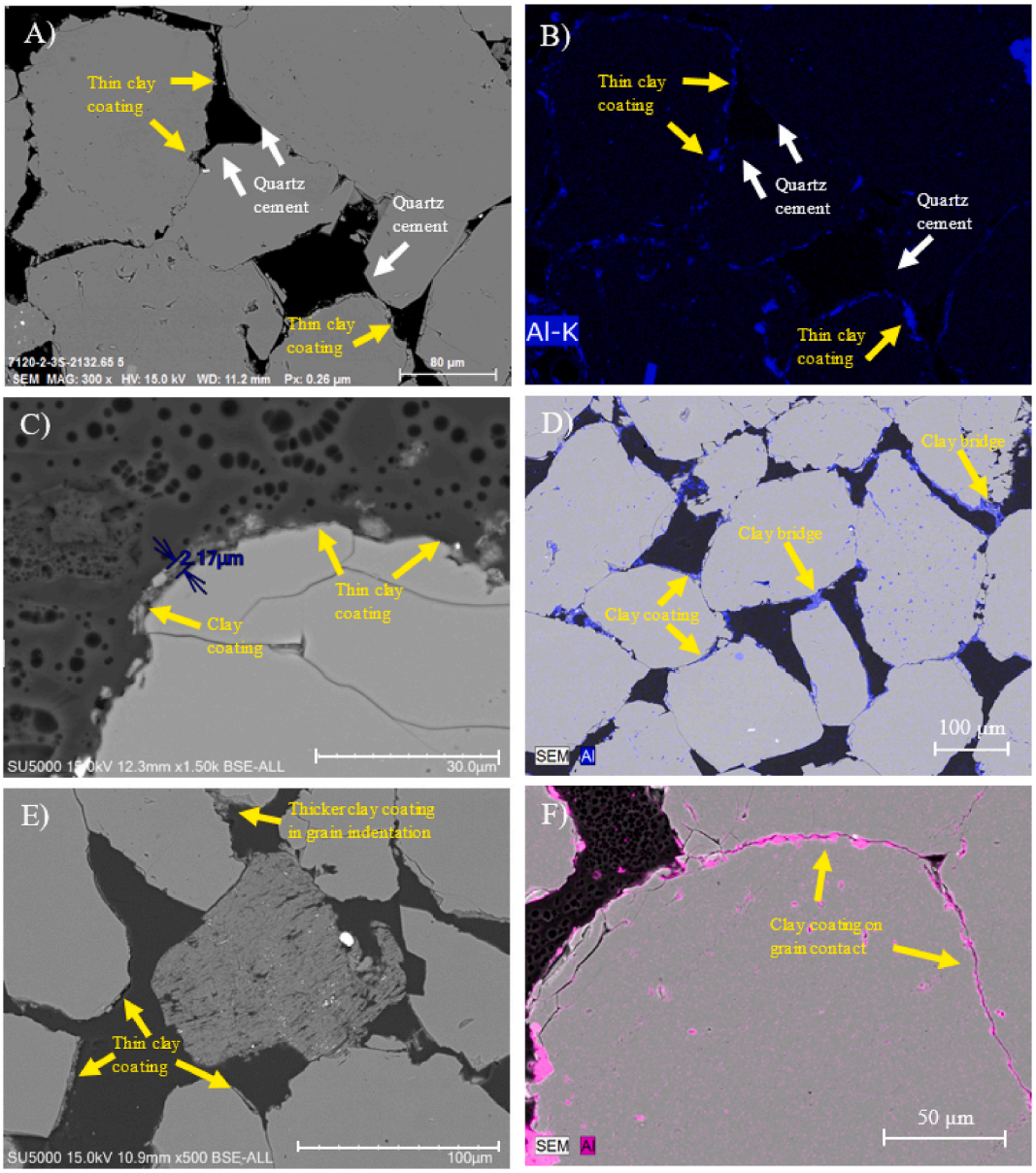

Fig. 5. A,B) Well 7120/2-3 S, sample 2132.65. SEM backscatter micrograph to the left and elemental mapping showing the aluminum on the right. Example of an area in the sample with variable coating coverage. Where coating is absent quartz cement is observed on detrital grain surfaces (white arrows), while at surfaces with sufficient grains coating (yellow arrows) quartz overgrowth is absent. C) 7120/6–1, sample 2446.26. Showing clay coating of varying thickness on quartz grain. The thicker part of the coating have a thickness of about 2 µm and shows that the clay particles are tangential to the quartz surface. D) Well, 7120/6–1 from sample 2461.80 MD. Coated sample. Note clay bridges between detrital grain framework. E) Well 7120/12–2, sample 1900.15 m. Note the varying thickness of the grain coating clay from grain indentations (yellow arrow) compared to general grain surfaces adjacent to the pore space. The thickness appears to me mostly governed by the surface texture of the detrital grains. F) Well 7119/9–1, sample 2760.50 MD. Elemental mapping showing the presence of Aluminum. The example show that clay is present on grain contacts. (For interpretation of the references to color in this figure legend, the reader is referred to the Web version of this article.)

had a high degree of grain coat coverage (Fig. 4 A-C and D-F). Other samples showed only remnants of grain coats and they were mainly characterized by abundant quartz cement (Fig. 4G–I). The grain coats exhibit a chaotic appearance (Fig. 5C) with an undulating outer rim and with a tendency to be patchy in some samples (Fig. 4 A-C and Fig. 5 A and B), while the grain coats are more continuous in other places (Fig. 4D–F). Another observation is that clay bridges are typically also seen in samples defined as coated (Fig. 5 D). When present, the grain coats are in most cases 1–4 µm thick (Fig. 5 C), but where indentations in the detrital grains exists, the thickness of grain coats can be significantly thicker (Fig. 5 E). Grain coats are also present at most detrital grain contacts in samples with a significant amount of grain coats (Fig. 4 A-F and Fig. 5 F). The contacts between detrital quartz grains in coated samples are often sutured (e.g., Fig. 4 A), indicating that the presence of grain coats facilitates quartz dissolution at the detrital quartz-clay interface at points of grain contact.

Based on the petrographic results, the quartz cement content was plotted against the IGV and porosity in order to investigate factors related to the grain coating illitic clay (Fig. 6 A and B). The intergranular volume (IGV) varies from as low as 20%–35% in the point counted samples. The results indicate that the IGV is generally lower in samples where significant grain coats have been observed (Fig. 6A, Table 2). The results also show that samples with grain coats have lower quartz cement volumes (Fig. 4 A and D compared to G, Fig. 6B) -, higher

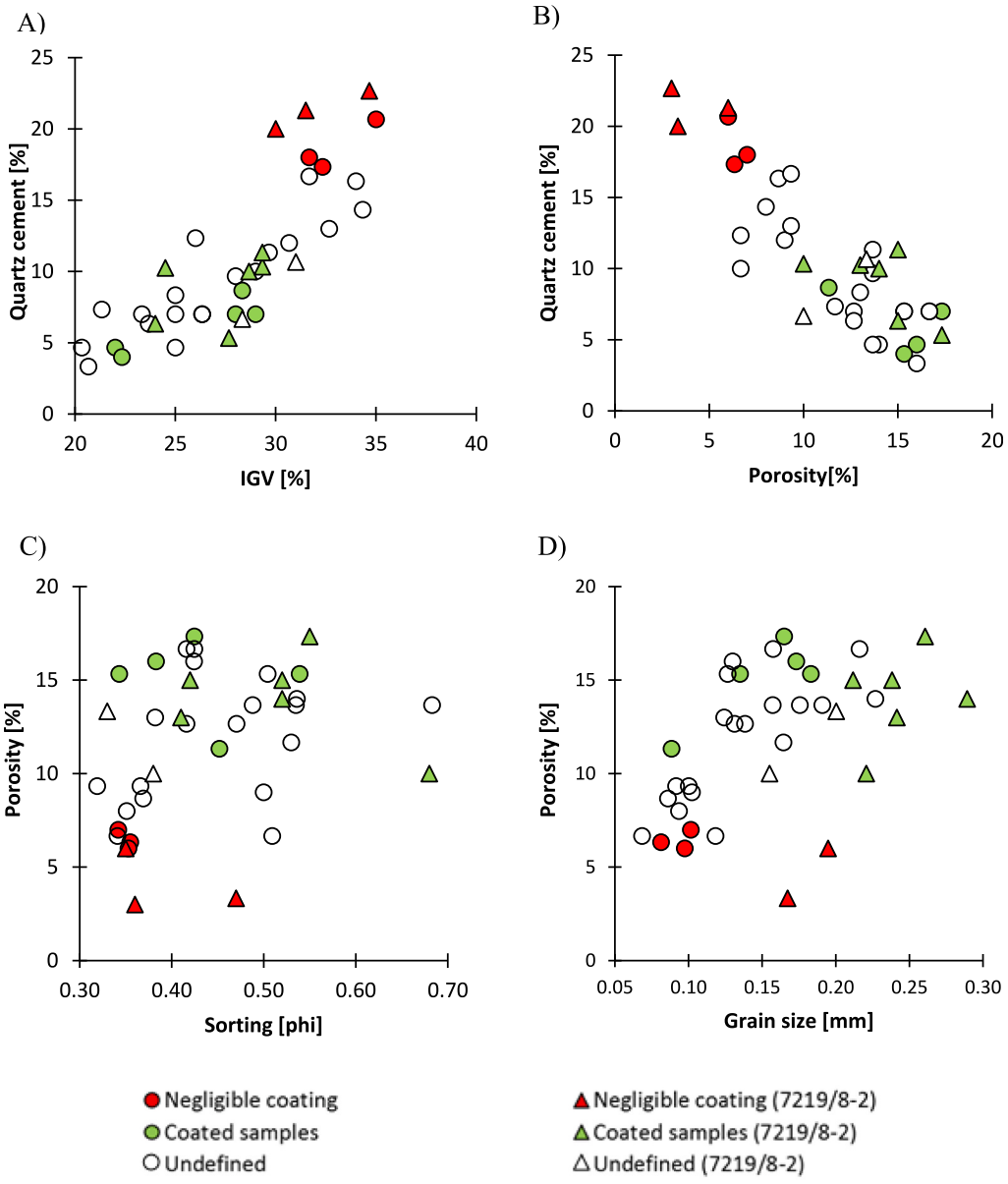

Fig. 6. Relations between various point count- and textural data obtained from thin section samples (See Table 2). A) Quartz cement vs IGV. B) Quartz cement vs. Porosity, C) Porosity vs. sorting. D) Porosity vs. grain size, triangular points represent data points from well 7219/8–2 from Hansen et al. (2017), while circular points represent data points obtained in this study. All samples are labeled as either a coated sample (green), negligible coated sample (red) or undefined (white) with the latter representing samples that were not investigated in the SEM. (For interpretation of the references to color in this figure legend, the reader is referred to the Web version of this article.)

porosities (Fig. 6B) –, a slightly poorer sediment sorting and a coarser grain size (Fig. 6C and D) compared to samples with negligible grain coating. Especially, there seems to be a strong relation between the observed quartz cement volume and IGV, where a gradual increase in quartz cement volumes favors a higher IGV. These observations agree with results from the reference well 7219/8–2 (Fig. 6 A and B).

4.3. Porosity, sonic velocity (Vp) and density

It is important to determine the relationship between core plug porosity, calculated porosity and the petrophysical characteristics of the sediments with abnormally high porosities. This will aid the possibility of detecting intervals with abnormally high porosities in wells or parts of the formation without petrographic control. A porosity line was calculated within the Stø Formation in all wells in order to obtain an accurate and continuous porosity estimate throughout the entire formation. Based on wells with petrographic control a cutoff value of 15% porosity was chosen (shaded area in Fig. 7A) for the calculated porosity curve in order to evaluate intervals without petrographic data that are likely to have effective grain coats within the Stø Formation. Fig. 7B shows a cross plot of core-plug porosity and the calculated neutron-density porosity and shows a strong correlation between the two. In the reference well 7219/8–2, a porosity cutoff value of 15% coincides with the interval proven to be significantly coated (Hansen et al., 2017). Although a threshold porosity of 15% in the wells from the Hammerfest basin (7121/5–1, 7120/6–1 and 7120/2-3 S) allow intervals with less petrographic certainty to be defined as possibly coated intervals, it successfully includes regions where grain coats have been proven and reject intervals where grain coating was observed to be negligible (Fig. 7A). Where the Stø Formation have undergone less – or more

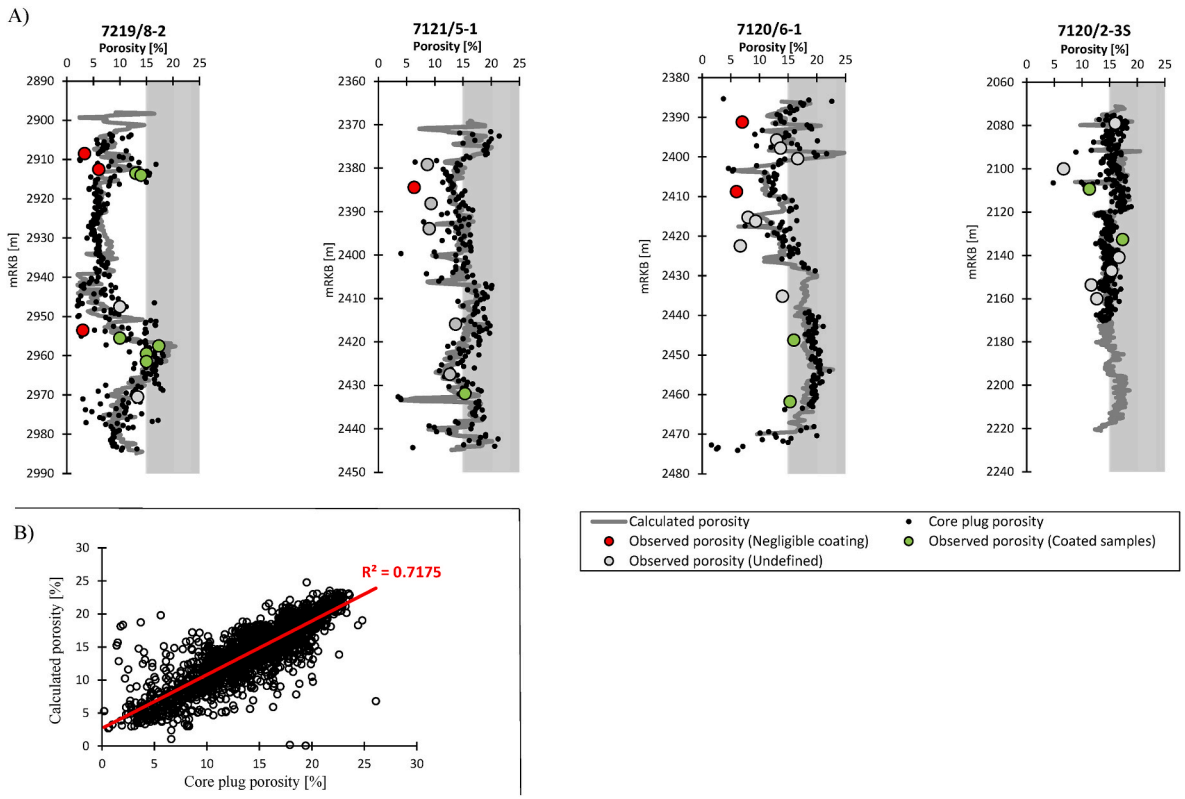

Fig. 7. A) Core plug – and calculated porosity trends for the Stø formation in the wells with point count results. Circles are point counted intergranular porosity colored with the SEM classification of the presence or absence of clay coating as defined in the legend. Undefined samples were not classified in SEM in regard to coating. B) Coreplug porosity versus calculated porosity for the studied wells. The calculated porosity shows a good match to the core plug porosity, especially for higher porosities (>12). For the lower porosities, the calculated porosities are in cases too high, most often caused by a higher content of clay.

burial, the cutoff value should be changed according to the porosity-depth trend in order to more accurately identify abnormally high porosity intervals in each individual well.

The data points are then filtered into two groups based on the cutoff porosity. The high porosity interval in well 7219/8–2 (Fig. 8A), shown to be significantly grain coated, have a whole rock density in the range of 2.25–2.38 g/cm^3 and a P-wave velocity ranging from approximately 3750 m/s to 4400 m/s. The density and P-wave velocity in the sub-population of porosities less than 15% gradually increases towards a density of approximately 2.62 g/cm^3 and a velocity exceeding 5000 m/s. The wells with petrographic data from the Hammerfest Basin (Fig. 8B), shows a similar trend, separating between high and low porosity intervals in the Vp-density domain. However, some of the data points of the higher porosities show elevated density readings (exceeding 2.4 g/cm^3). This is most likely reflecting intervals with a slightly higher amount of pore filling clays. Finally, a cross plot of all available density and P-wave velocity data in this study (reference well 7219/8–2 not included) shows the acoustic response from the Stø Formation in the study area (Fig. 8C). The results show that there is a significant spread in velocities both for intervals with porosity greater than 15% and intervals with porosity less than 15%. In terms of density, the intervals show an expected trend where intervals with higher porosity have a lowered density and vice versa.

4.4. Porosity distribution

All helium porosity data from within the Stø Formation in all wells included in the study can be seen in Fig. 9. The core plug porosity distribution often shows abnormal subpopulations of both higher and lower porosities deviating from a normal distribution of porosites. The sub-populations of abnormally low porosites almost exclusively correlates to high density calcite cemented layers. The sub-populations of abnormally high porosities coincide with intervals of grain coats in all four wells where petrographic data were available.

4.5. Porosity depth trend

Excluding the parts of the Stø Formation with a Vshale content above 20%, the Stø Formation still show a large spread in porosity values in each of the studied wells (Fig. 10 A). The spread in the porosity distribution for a given depth level is observed to increase with increasing burial depths. The parts of the Stø Formation in the different wells assumed to consist of clean, i.e., less than 10% clay by volume, well cemented non coated sands shows a high degree of compaction with depth in the chemical compaction domain and is likely to plot closer to the red line (Fig. 10 A). The cleaner parts of the formation assumed to consist of clean, well-coated sands with less quartz cement compact less with increasing depth and will plot closer to the green line (Fig. 10 A). This is also supported by the core plug porosity depth trend colored with P-sonic data (Fig. 10 B) that indicates that sonic velocity fluctuations vary systematically with change in porosity.

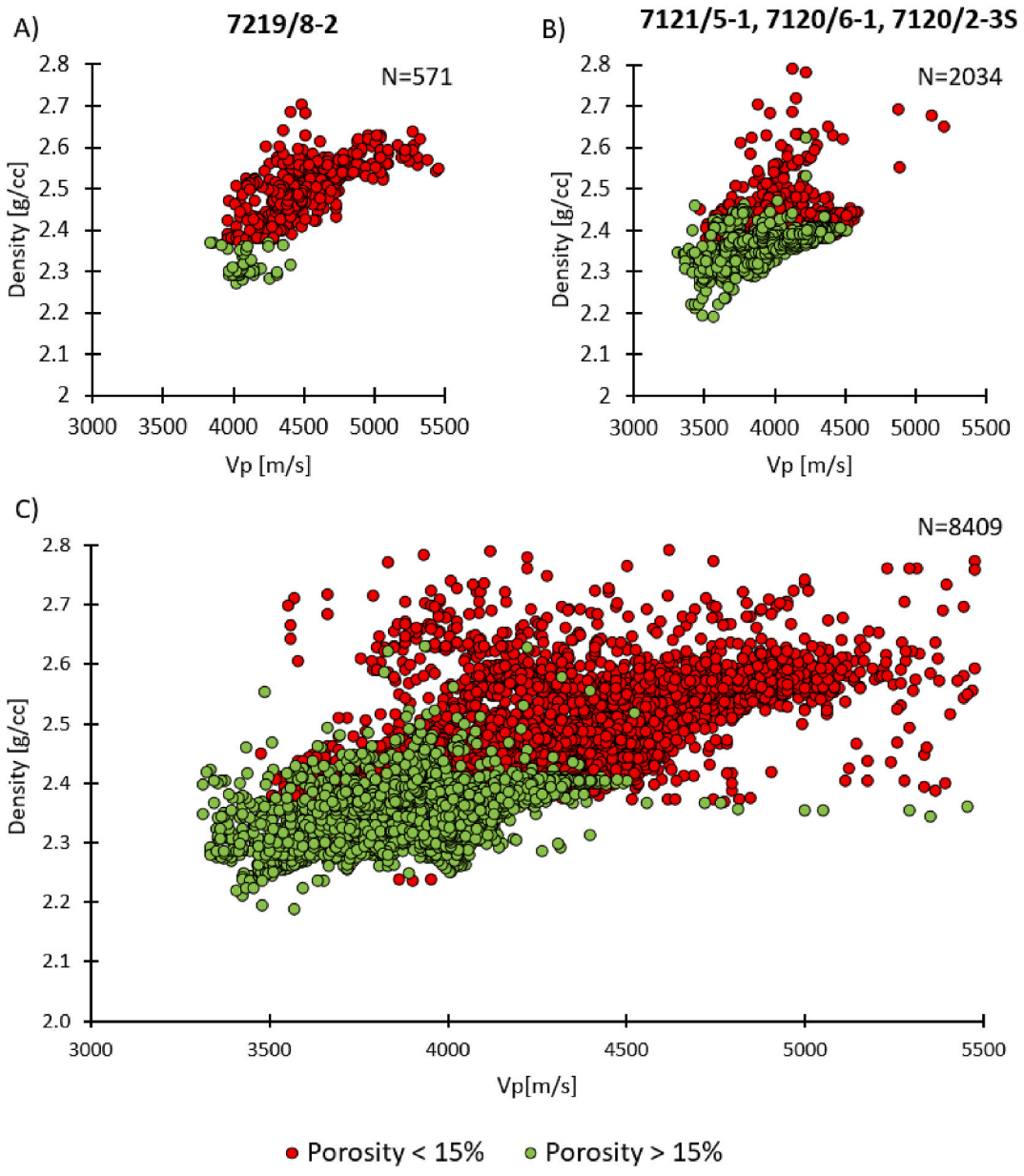

Fig. 8. Vp-density crossplots for the Stø formation in well 7219/8–2 (A), 7121/5–1, 7120/6–1 and 7120/2-3 S (B) and for all the wells in the study (C).

5. Discussion

The petrographic (Fig. 4) and textural parameters (Fig. 5) of the Stø Formation in wells 7121/5–1, 7120/6–1 and 7120/2–3 in the Hammerfest Basin are similar to those recognized in the reference well 7219/8–2, located in the Bjørnøyrenna Fault Complex (Hansen et al., 2017). This uniform composition of the sediments and the widespread occurrence of grain coats of an illitic composition found regionally within the Stø Formation in all the studied wells (Table 2) indicates that similar depositional conditions and grain coat emplacing processes have taken place over large areas. The process (es) resulting in the original emplacement of precursor clay on detrital grains in the Stø Formation is not possible to conclude from the data presented in this paper. Hence, detailed sedimentological- and experimental studies should be conducted to investigate this further. However, the study has shown that delicate features like clay bridges between detrital grains and a slightly better sediment sorting can be observed in coated intervals, while remnants of grain coats can be observed in intervals with negligible coating. This could indicate that whatever process responsible for the emplacement of the coating was common throughout the development of this very condensed section, but where the balance between this process and the amount of sediment reworking subsequently controlled the extent of precursor grain coats.

The results show that there is an overall strong positive correlation between IGV and quartz cement content (Fig. 6A) and a strong negative correlation between quartz cement and porosity (Fig. 6B). The coated

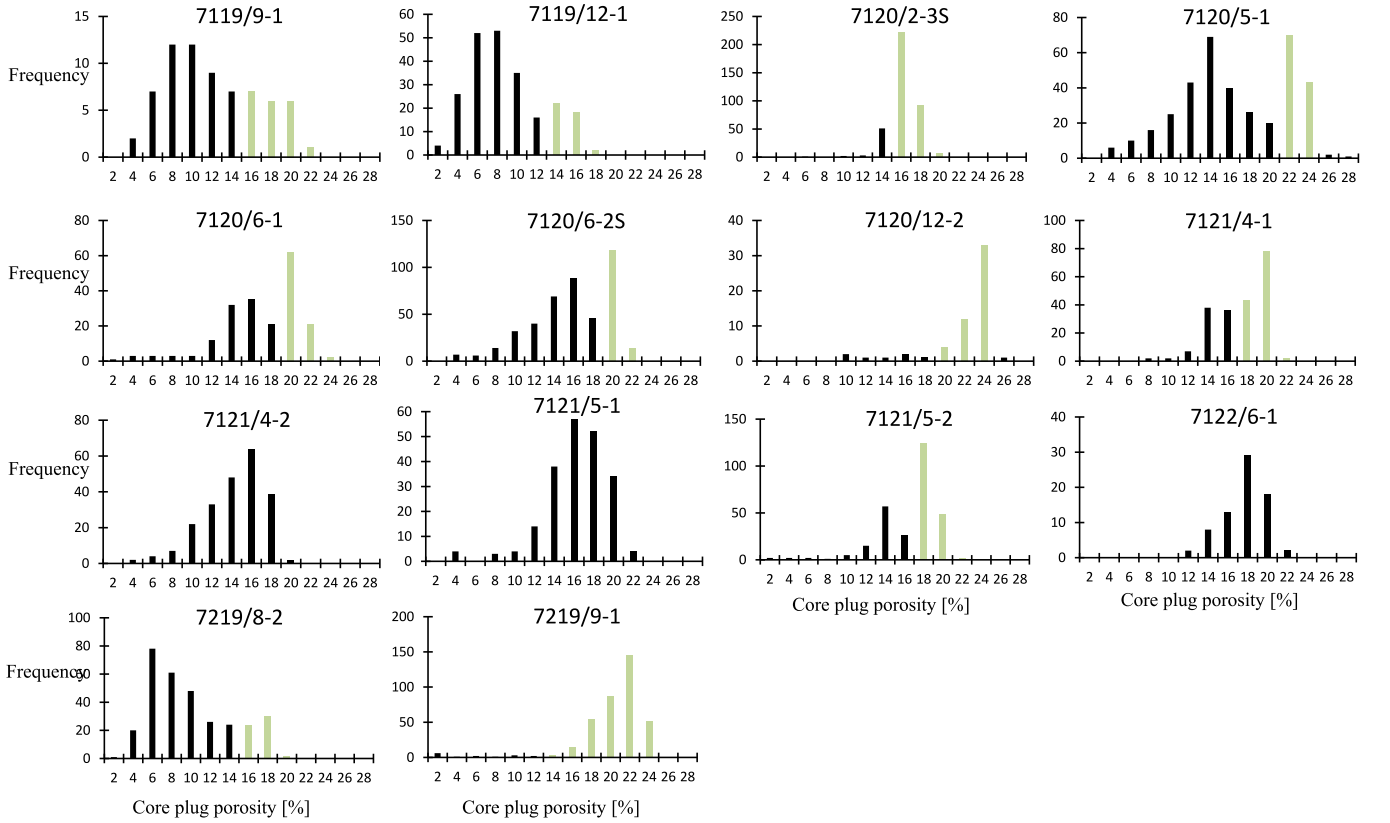

Fig. 9. Core plug porosity data from all 14 wells included in the study. Green bars highlight wells with a clear subpopulation of abnormally high porosities. (For interpretation of the references to color in this figure legend, the reader is referred to the Web version of this article.)

samples are characterized by a lower IGV and a lower amount of quartz cement compared to samples with negligible grain coats. Grain coating illitic clay will to some extent reduce the IGV, and porosity, of the sediments due to a clay induced dissolution process (CID) acting at points of contact between the detrital quartz grains (Bjørkum, 1996). This means that too extensive illitic clay coating could have a negative effect on the reservoir quality and should be taken into consideration. However, the total amount of illitic clay in the Stø Formation is generally not enough to cause this to be a major factor in the resultant porosity. The grain coats limits the amount of chemical compaction in these well-coated intervals (Fig. 4A–F) as the illitic clay decreases the available nucleation area for quartz cement (Walderhaug, 1994). The strong correlation between IGV and amount of quartz cement (Fig. 6A) in samples with grain coats are therefore likely to represent the combined effect of quartz cement retardation and the effect of microstylolitization with quartz cementation being the major factor. In addition, continued mechanical compaction due to low initial quartz cement volumes during early chemical compaction may also be responsible for reducing the IGV to a certain degree in well coated intervals. However, substantial mechanical compaction within the chemical compaction domain would likely only take place in intervals with an exceedingly continuous grain coating coverage. In intervals where grain coating illite is negligible (Fig. 4G–I) the IGV is likely to be kept constant, i.e., representing the IGV as it was just after onset of quartz cementation and further mechanical compaction is prevented. In such cases detrital quartz grains is mainly dissolved along macroscopic stylolites acting as a silica source for quartz cement growth within the volume between the stylolites (Walderhaug, 1996). It is also important to underline that the low quartz cement volume in intervals with abundant grain coats are not likely to be a result of insufficient silica concentrations. All points of contact between a quartz grain and the illitic clay or mica grain, whether emplaced as coating or pore-filling clays, can be a source of silica (Bjørkum, 1996; Walderhaug, 1996). Hansen et al. (2017) also observed that intragranular cracks in detrital quartz grains were filled with quartz cement within intervals with grain coats. This indicate that sufficient silica supersaturation for quartz cement growth was present also in sections of the Stø Formation with grain coats and little quartz cement overgrowth. Moreover, samples with extensive coating coverage have higher porosities but a lower IGV (Fig. 6A, C and D). In terms of textural properties, the samples with extensive coating coverage have slightly coarser grain sizes and poorer sorting (Fig. 6C and D). Coarser grained and poorer sorted sediments are prone to compact more mechanically (Chuhan et al., 2002), and this could to some extent explain the lower IGV values in these samples. However, the higher porosities in these samples indicates that the differences in textural parameters are not the main controlling factor on porosity distribution in deeply buried parts of the Stø Formation, but rather the amount of quartz cement which is controlled by coating coverage. The porosity distribution plots seen in Fig. 9 shows that the normally distributed population of porosities is centered around a mean value consistent with the porosity depth trend of clean uncoated shallow marine sands (Marcussen et al., 2010). However there are several subpopulations of porosities in the Stø Formation that are abnormally high. The porosity depth trend for the Stø Formation in the 14 studied wells is shown in Fig. 10. The depths have

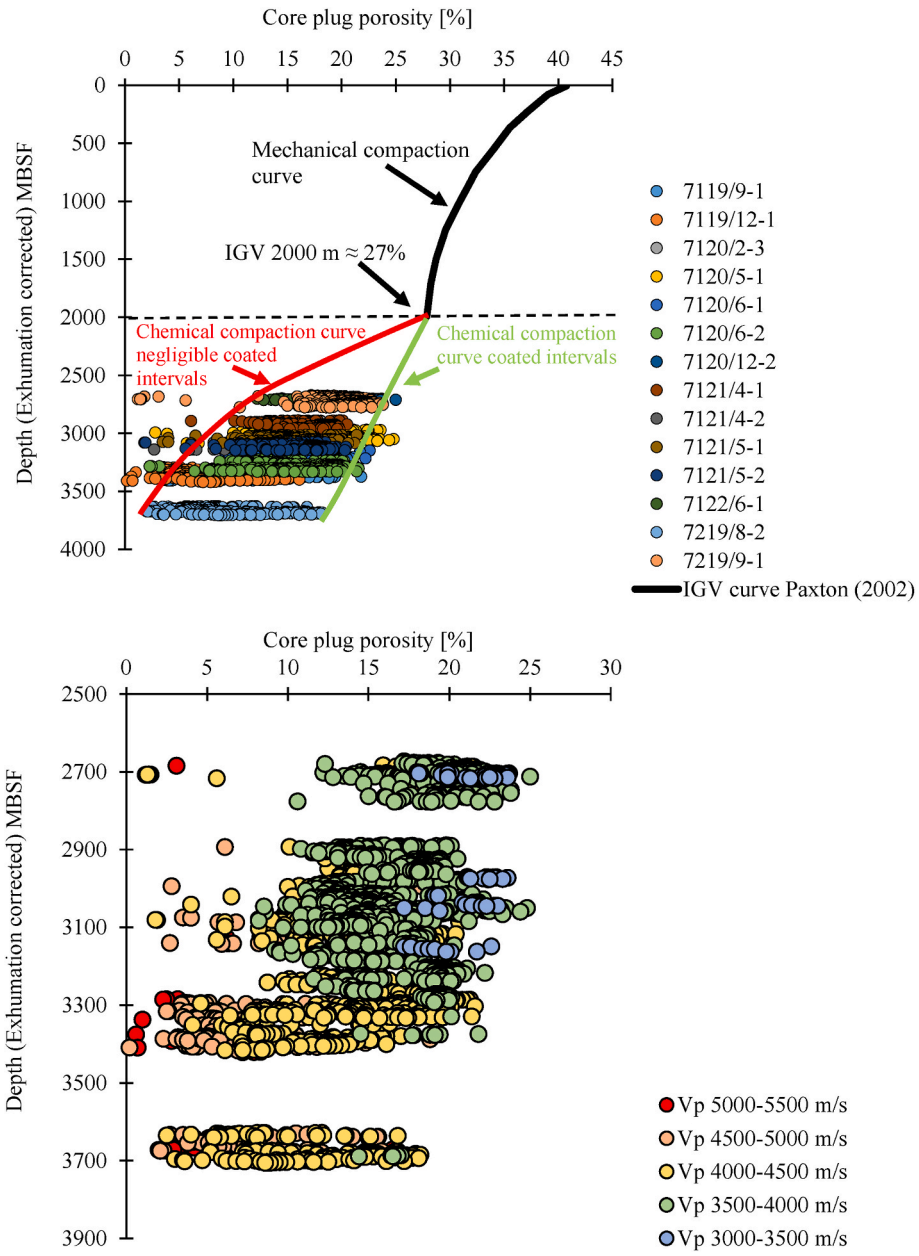

Fig. 10. The porosity depth trend for the Stø Formation in all the studied wells with exhumation corrected depths. Only sands with an estimated Vshale of less than 20% are plotted. Note the higher rate of porosity decrease with depth for the lower porosities. A) Data colored with well names. The plot also shows the IGV curve of Paxton et al. (2002) which could be a likely mechanical compaction evolution for all the clean sandstone intervals of the Stø Formation. At the onset of the quartz cementation, results show that intervals within the Stø Formation is likely to follow quite different compaction trends, depending on the clay coating coverage. B) Data colored with Vp. The plot concentrates on the porosity depth interval from 2500 m and illustrates the difference in compaction rate between the higher and lower porosity intervals within the Stø Formation.

been corrected for exhumation and since porosity reduction is largely a non-reversible process the data closely represents the real depth trend of the formation. Any differences in textural and mineralogical composition (size, sorting, clay content etc.) will cause variations in porosity due to varying response to increased mechanical compaction, but due to the homogenous nature of the Stø Formation (Table 2) the depth trend within the mechanical compaction domain will likely be similar across the formation (e.g., Fawad et al., 2011), exemplified here by the Paxton et al. (2002) compaction line in Fig. 10 A. The amount of quartz cement will be by far the most important factor controlling porosity within each depth interval in the chemical compaction domain. Since the TTI can be assumed to be relatively uniform for all the wells studied, higher porosities would reflect lower quartz cement volumes within some sections of the Stø Formation due to coating. The spread in porosity i.e., the range of porosity values in the clean intervals of the Stø Formation is clearly seen to increase with depth (Fig. 10). This is in accordance with what is expected from the rate of silica precipitation, governed by the TTI, with a significant increase in the rate of silica precipitation with higher temperatures (Walderhaug, 1996). The uncoated parts of the Stø formation will therefor loose porosity at an ever-increasing rate compared to the coated sands in the chemical compaction domain (Fig. 10). Even the intervals with the highest degree of grain coating coverage compact more than what would be the case if compaction were a function of mechanical compaction only, showing that some precipitation of quartz cement takes place even in the sediments with the highest degree of grain coating coverage (Fig. 10 B). The most extreme difference in rate of compaction in coated- and negligible coated intervals within the Stø Formation can be represented by hypothetical compaction lines following the upper – and lower porosity limit as a function of depth (Fig. 10). This result agrees with the model of Ajdukiewicz and Lander (2010) (Fig. 1) and fits well with SEM observations showing that in most cases the coating does not completely cover the detrital grains, allowing some quartz cement formation (e.g., Fig. 5 A and B).

The Stø Formation in all the studied wells have been subjected to burial depths well within the temperature range required for quartz cementation pre uplift, but there is a large variation in the amount of

quartz cement in what is otherwise similar sediments both in respect to composition and burial history. The homogenous nature of the sediment composition of the Stø Formation makes it especially interesting to understand the relationship between the varying amount of quartz cement and the corresponding variations in sonic velocity and bulk density in order to see if possibly coated intervals at various depths are easily detectable by petrophysical data alone. The strong correlation between the computer processed interpretation (CPI) porosity curves and core plug data (Fig. 7) allowed for the well log data to be included in the characterization of the elastic parameters with higher confidence (Fig. 8). For the wells with petrographic control studied here, a cutoff porosity of 15% coincide well with coated intervals having porosities higher than this, and less coated intervals having lower porosities (Fig. 7 A). The widespread distribution of data points in the Vp-density domain (Fig. 8) is likely a result of several different factors that are difficult to accurately account for and includes the type of fluid saturating the rock, porosity, mineralogical composition and calibration and type of tools used to acquire the elastic parameters. However, the results indicate that coated and negligible coated intervals should be distinguishable in the Vp-density domain (Fig. 8). The link between the petrographic- and petrophyscial data established herein also indicate that these two types of intervals are common on a regional scale in this formation. This means that it may be possible to infer reservoir quality within deeply buried parts of the Stø Formation on a regional scale using only basic well logs due to the different rate of compaction in intervals with effective grain coats vs-negligible coated intervals. Hence, powerful predictive models could likely be established without the need for expensive petrographic- or core plug data within the Stø Formation.

6. Conclusion

14 wells containing the Stø Formation from the Hammerfest basin and Bjørnøyrenna Fault Complex were studied to investigate the regional occurrence of grain coating illitic clay and its control on the porosity distribution in deeply buried parts of the formation. Grain coating clay is observed in the potentially good reservoir sands of the Stø Formation in all the studied wells, indicating that the emplacement of grain coating illitic clay is common on a large regional scale. The extent of the grain coating coverage on the detrital grains however is highly varying and only some intervals are seen to have extensive grain coats enough to significantly inhibit quartz cementation and preserve abnormally high porosities. The Stø Formation is largely homogenous and although variations in mineralogical and textural parameters are present, the amount of grain coating coverage is the main factor in controlling porosities in deeply buried parts of the formation. With increasing burial depths, an ever-wider porosity distribution will be caused by the massively different rate of quartz cementation between intervals with significant coating coverage and those with negligible coating coverage. The large difference in the compaction trend between intervals with significant grain coat coverage and those with less consistent grain coats could allow for easy generation of predictive models without the need for expensive petrographic- or core plug data.

Declaration of competing interest

The authors declare that they have no known competing financial interests or personal relationships that could have appeared to influence the work reported in this paper.

Acknowledgements

The authors would like to acknowledge the valuable assistance of Siri Simonsen in the SEM analysis performed for this study, and Salahalldin Akhavan for the preparations of the thin sections. The PhD scholarship-funding support the second author, Department of Geosciences, UiO. We would furthermore like to express our gratitude to our wonderful colleagues at the department for valuable discussions and suggestions.

References

Aase, N.E., Bjørkum, P.A., Nadeau, P.H., 1996. The role of grain-coating microquartz on preservation of reservoir porosity. AAPG (Am. Assoc. Pet. Geol.) Bull. 80 (10), 1654–1673.

Ajdukiewicz, J.M., Lander, R.H., 2010. Sandstone reservoir quality prediction; the state of the art. AAPG (Am. Assoc. Pet. Geol.) Bull. 94, 1083–1091. https://doi.org/10.1306/intro060110.

Baig, I., Faleide, J.I., Jahren, J., Mondol, N.H., 2016. Cenozoic exhumation on the southwestern Barents Shelf: estimates and uncertainties constrained from compaction and thermal maturity analyses. Mar. Petrol. Geol. 73, 105–130. https://doi.org/10.1016/j.marpetgeo.2016.02.024.

Bergan, M., Knarud, R., 1993a. Apparent changes in clastic mineralogy of the Triassic-Jurassic succession, Norwegian Barents Sea; possible implications for palaeodrainage and subsidence. Norwegian Pet. Soc.confer. Arctic geol pet. potential 2, 481–493.

Bergan, M., Knarud, R., 1993b. Apparent Changes in Clastic Mineralogy of the Triassic–Jurassic Succession, Norwegian Barents Sea: Possible Implications for Palaeodrainage and Subsidence, vol. 2. Norwegian Petroleum Society Special Publications, pp. 481–493. https://doi.org/10.1016/B978-0-444-88943-0.50034-4.

Bjørkum, P.A., 1996. How important is pressure in causing dissolution of quartz in sandstones? J. Sediment. Res. 66, 147–154. https://doi.org/10.1306/D42682DE-2B26-11D7-8648000102C1865D.

Bjørlykke, K., 1998. Clay mineral diagenesis in sedimentary basins - a key to the prediction of rock properties. Examples from the North Sea Basin. Clay Miner. 33, 14–34.

Bjørlykke, K., Egeberg, P.K., 1993. Quartz cementation in sedimentary basins. AAPG (Am. Assoc. Pet. Geol.) Bull. 77 (9), 1538–1548.

Bjørlykke, K., Ramm, M., Saigal, G.C., 1989. Sandstone diagenesis and porosity modification during basin evolution. Geol. Rundsch. 78, 243–268. https://doi.org/10.1144/GSL.SP.1992.061.01.15.

Chuhan, F.A., Kjeldstad, A., Bjørlykke, K., Høeg, K., 2002. Porosity loss in sand by grain crushing—experimental evidence and relevance to reservoir quality. Mar. Petrol. Geol. 19, 39–53. https://doi.org/10.1016/S0264-8172(01)00049-6.

Dutton, S.P., Diggs, T.N., 1992. Evolution of porosity and permeability in the lower cretaceous travis peak formation, east Texas. AAPG Bull. 76, 252–269.

Ehrenberg, S.N., 1993. Preservation of anomalously high porosity in deeply buried sandstones by grain-coating chlorite: examples from the Norwegian Continental Shelf. AAPG (Am. Assoc. Pet. Geol.) Bull. 77, 1260–1286. https://doi.org/10.1306/BDFF8E5C-1718-11D7-8645000102C1865D.

Fawad, M., Mondol, N.H., Jahren, J., Bjørlykke, K., 2011. Mechanical compaction and ultrasonic velocity of sands with different texture and mineralogical composition. Geophys. Prospect. 59, 697–720. https://doi.org/10.1111/j.1365-2478.2011.00951.x.

Folk, R.L., Ward, W.C., 1957. Brazos River bar [Texas]; a study in the significance of grain size parameters. J. Sediment. Res. 27, 3–26.

Gjelberg, J., Dreyer, T., Høie, A., Tjelland, T., Lilleng, T., 1987. Late triassic to mid-jurassic sandbody development on the Barents and mid-Norwegian shelf. In: BROOKS, J., GLENNIE, K.W. (Eds.), Petroleum Geology of North West Europe. Geological Society, London, pp. 1105–1129.

Griffiths, J., Worden, R.H., Wooldridge, L.J., Utley, J.E., Duller, R.A., 2018. Detrital clay coats, clay minerals, and pyrite: a modern shallow-core analogue for ancient and deeply buried estuarine sandstones. J. Sediment. Res. 88, 1205–1237. https://doi.org/10.2110/jsr.2018.56.

Haile, B.G., Klausen, T.G., Czarniecka, U., Xi, K., Jahren, J., Hellevang, H., 2018. How are diagenesis and reservoir quality linked to depositional facies? A deltaic succession, Edgeøya, Svalbard. Mar. Petrol. Geol. 92, 519–546.

Hansen, H.N., Løvstad, K., Müller, R., Jahren, J., 2017. Clay coating preserving high porosities in deeply buried intervals of the Stø Formation. Mar. Petrol. Geol. 88, 648–658.

Heald, M.T., Larese, R.E., 1974. Influence of coatings on quartz cementation. J. Sediment. Petrol. 44 (4), 1269–1274.

Jahren, J., Ramm, M., 2000. The porosity-preserving effects of microcrystalline quartz coatings in arenitic sandstones: examples from the Norwegian continental shelf. Quartz Cementation in Sandstones 271–280.

Klausen, T.G., Müller, R., Sláma, J., Olaussen, S., Rismyhr, B., Helland-Hansen, W., 2018. Depositional history of a condensed shallow marine reservoir succession: stratigraphy and detrital zircon geochronology of the Jurassic Stø Formation, Barents Sea. J. Geol. Soc. 175, 130–145. https://doi.org/10.1144/jgs2017-024.

Klausen, T.G., Müller, R., Poyatos-Moré, M., Olaussen, S., Stueland, E., 2019. Tectonic, provenance and sedimentological controls on reservoir characteristics in the upper triassic–middle jurassic realgrunnen subgroup, SW Barents Sea. Geol. Soc. Spec. Publ. 495, 2018–2165. https://doi.org/10.1144/SP495-2018-165.

Line, L.H., Jahren, J., Hellevang, H., 2018. Mechanical compaction in chlorite-coated sandstone reservoirs–examples from middle–late triassic channels in the southwestern Barents Sea. Mar. Petrol. Geol. 96, 348–370.

Line, L.H., Müller, R., Klausen, T.G., Jahren, J., Hellevang, H., 2020. Distinct petrographic responses to basin reorganization across the Triassic–Jurassic boundary in the southwestern Barents Sea. Basin Res. 1–22. https://doi.org/10.1111/bre.12437, 00.

Lundegard, P.D., 1992. Sandstone porosity loss - a "big picture' view of the importance of compaction. J. Sediment. Petrol. 62 (2), 250–260.

Maast, T.E., Jahren, J., Bjørlykke, K., 2011. Diagenetic controls on reservoir quality in middle to upper jurassic sandstones in the south viking graben, North SeaDiagenetic controls on reservoir quality in the south viking graben sandstones. AAPG Bull. 95, 1883–1905.

Marcussen, Ø., Maast, T.E., Mondol, N.H., Jahren, J., Bjørlykke, K., 2010. Changes in physical properties of a reservoir sandstone as a function of burial depth – the Etive Formation, northern North Sea. Mar. Petrol. Geol. 27, 1725–1735. https://doi.org/10.1016/j.marpetgeo.2009.11.007.

Matlack, K.S., Houseknecht, D.W., Applin, K.R., 1989. Emplacement of clay into sand by infiltration. J. Sediment. Res. 59, 77–87. https://doi.org/10.1306/212F8F21-2B24-11D7-8648000102C1865D.

Mcbride, E.F., 1989. Quartz cement in sandstones: a review. Earth Sci. Rev. 26, 69–112.

Müller, R., Klausen, T.G., Faleide, J.I., Olaussen, S., Eide, C.H., Suslova, A., 2019. Linking regional unconformities in the Barents Sea to compression-induced forebulge uplift at the Triassic-Jurassic transition. Tectonophysics 765, 35–51.

Needham, S., Worden, R., Mcilroy, D., Needham, S., 2005. Experimental production of clay rims by macrobiotic sediment ingetion and excretion processes. J. Sediment. Res. 75, 1028–1037. https://doi.org/10.2110/jsr.2005.078.

Olaussen, S., Dalland, A., Gloppen, T.G., Johannessen, E., 1984. Depositional environment and diagenesis of Jurassic reservoir sandstones in the eastern part of Troms I area. In: SPENCER, A.M. (Ed.), Petroleum Geology of the North European Margin: Proceedings of the North European Margin Symposium (NEMS '83), Organized by the Norwegian Petroleum Society and Held at the Norwegian Institute of Technology (NTH) in Trondheim 9–11 May, 1983. Springer Netherlands, Dordrecht.

Paxton, S.T., Szabo, J.O., Ajdukiewicz, J.M., 2002. Construction of an intergranular volume compaction curve for evaluating and predicting compaction and porosity loss in rigid-grain sandstone reservoirs. AAPG (Am. Assoc. Pet. Geol.) Bull. 86, 2047–2065.

Ramm, M., Forsberg, A.W., Jahren, J.S., 1997. Porosity-depth trends in deeply buried upper jurassic reservoirs in the Norwegian central graben: an example of porosity preservation beneath the normal economic basement by grain-coating microquartz. In: KUPECZ, J.A., GLUYAS, J., BLOCH, S. (Eds.), Reservoir Quality Prediction in Sandstones and Carbonates, vol. 69. AAPG Memoir, pp. 177–199.

Ryseth, A., 2014. Sedimentation at the jurassic-triassic boundary, south-west Barents Sea: indication of climate change. In: MARTINIUS, A.W., RAVNÅS, R., HOWELL, J. A., STEEL, R.J., WONHAM, J.P. (Eds.), From Depositional Systems to Sedimentary Successions on the Norwegian Continental Margins. John Wiley & Sons, Ltd, Chichester, UK.

Storvoll, V., Bjørlykke, K., Karlsen, D., Saigal, G., 2002. Porosity preservation in reservoir sandstones due to grain-coating illite: a study of the Jurassic Garn Formation from the Kristin and Lavrans fields, offshore Mid-Norway. Mar. Petrol. Geol. 19, 767–781. https://doi.org/10.1016/S0264-8172(02)00035-1.

Virolle, M., Brigaud, B., Bourillot, R., Féniès, H., Portier, E., Duteil, T., Nouet, J., Patrier, P., Beaufort, D., 2019. Detrital clay grain coats in estuarine clastic deposits: origin and spatial distribution within a modern sedimentary system, the Gironde Estuary (south-west France). Sedimentology 66, 859–894. https://doi.org/10.1111/sed.12520.

Walderhaug, O., 1994. Precipitation rates for quartz cement in sandstones determined by fluid-inclusion microthermometry and temperature-history modeling. J. Sediment. Res. 64, 324–333.

Walderhaug, O., 1996. Kinetic modeling of quartz cementation and porosity loss in deeply buried sandstone reservoirs. AAPG (Am. Assoc. Pet. Geol.) Bull. 80, 731–745. https://doi.org/10.1306/64ED88A4-1724-11D7-8645000102C1865D.

Wilson, M.D., 1992. Inherited grain-rimming clays in sandstones from eolian and shelf environments: their origin and control on reservoir properties. In: Origin, Diagenesis, and Petrophysics of Clay Minerals in Sandstones, vol. 47. SEPM Special Publication, pp. 209–225.

Wooldridge, L.J., Worden, R., Griffiths, J., Thompson, A., Chung, P., 2017a. Biofilm origin of clay-coated sand grains. Geology 45, 875–878. https://doi.org/10.1130/G39161.1.

Wooldridge, L.J., Worden, R.H., Griffiths, J., Utley, J.E., 2017b. Clay-coated sand grains in petroleum reservoirs: understanding their distribution via A modern analogue. J. Sediment. Res. 87, 338–352. https://doi.org/10.2110/jsr.2017.20.

Worsley, D., 2008. The post-caledonian development of svalbard and the western Barents Sea. Polar Res. 27, 298–317. https://doi.org/10.1111/j.1751-8369.2008.00085.x.

Worsley, D., Ofstad, K., Kristensen, S.E., 1988. The mesozoic and cenozoic succesion of tromsøflaket. In: DALLAND, A., WORSLEY, D., OFSTAD, K. (Eds.), A Lithostrategraphic Scheme for the Mesozoic and Cenozoic Succession Offshore Mid- and Northern Norway, vol. 4. Norwegian Petroleum Directorate Bulletin, pp. 42–65.